Magnetic Testing, and Modeling, Simulation and Analysis for Space Applications

Mary Boghosian*, Pablo Narvaez**, Ray Herman[1],

*The Aerospace Corporation, ** Jet Propulsion Laboratory, California Institute of Technology

ABSTRACT

The Aerospace Corporation (Aerospace) and Lockheed Martin Space Systems (LMSS) participated with Jet Propulsion Laboratory (JPL) in the implementation of a magnetic cleanliness program of the NASA/JPL JUNO mission. The magnetic cleanliness program was applied from early flight system development up through system level environmental testing. The JUNO magnetic cleanliness program required setting-up a specialized magnetic test facility at Lockheed Martin Space Systems for testing the flight system and a testing program with facility for testing system parts and subsystems at JPL. The magnetic modeling, simulation and analysis capability was set up and performed by Aerospace to provide qualitative and quantitative magnetic assessments of the magnetic parts, components, and subsystems prior to or in lieu of magnetic tests.

Because of the sensitive nature of the fields and particles scientific measurements being conducted by the JUNO space mission to Jupiter, the imposition of stringent magnetic control specifications required a magnetic control program to ensure that the spacecraft's science magnetometers and plasma wave search coil were not magnetically contaminated by flight system magnetic interferences. With Aerospace's magnetic modeling, simulation and analysis and JPL's system modeling and testing approach, and LMSS's test support, the project achieved a cost effective approach to achieving a magnetically clean spacecraft.

This paper presents lessons learned from the JUNO magnetic testing approach and Aerospace's modeling, simulation and analysis activities used to solve problems such as remnant magnetization, performance of hard and soft magnetic materials within the targeted space system in applied external magnetic fields.

KEY WORDS: magnetics, magnetic cleanliness, system magnetic testing, magnetic modeling and simulation

BACKGROUND

The JUNO spacecraft scientific fields and particles payload instrument included a magnetometer instrument that will be performing measurements both in interplanetary cruise and in Jupiter's magnetic field. The instrument consisted of two sensors; an Inboard Fluxgate Magnetometer sensor (IFGM) and an Outboard Fluxgate Magnetometer Sensor (OFGM). Both these sensors were mounted on a magnetometer boom platform whose closest edge was approximately 10 meters from the center of the spacecraft X-direction, with the IFGM located at about 10 meters,

[1] Formerly at The Aerospace Corporation. Current contact information is (310) 750-6772 or (562)896-7068

and the OFGM located at about 11 meters from the center of the spacecraft. Figure 1 represents an artist rendition of the JUNO spacecraft reference [1].

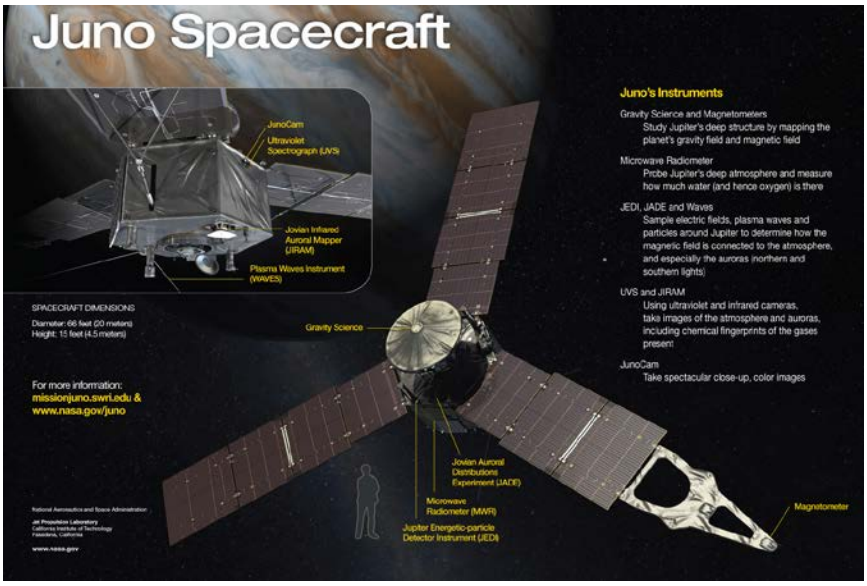

Figure 1- JUNO Spacecraft (Courtesy of NASA)

The magnetometers were mounted far from other spacecraft subsystems in order to take advantage of the inverse cube of the distance fall off of magnetic fields; however, the complex nature of the spacecraft indicated, early in the project, that the potential for magnetic contamination of the science magnetometers' magnetic field data was still a distinct possibility.
Early in the project phase, several spacecraft subsystems and science instruments were identified as potential magnetic interference sources. A survey performed revealed that the spacecraft's various subsystems would include highly magnetic parts and components, such as stepper motors, solar array linear boom actutator motors, traveling wave tube amplifiers (TWTAs), a number of highly magnetic propulsion system latch valves, RF isolators and circulators, RF waveguide switches, etc. Preliminary magnetic moment calculations, and modeling and simulations indicated that all of the permanent magnets contained in these highly magnetic subsystems and components could collectively have impact on the magnetometer science experiments by generating high residual magnetic fields at the IFGM, even when mounted approximately 10 meters from the spacecraft. Current loops were also controlled as described later. Figure 2 shows the locations of both IFGM and OFGM along the JUNO magnetometer boom platform.

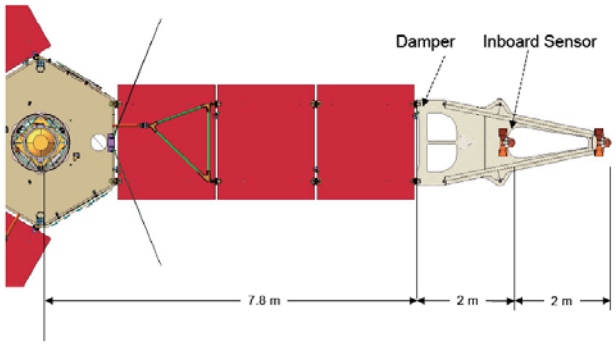

Figure 2 - JUNO Locations of the IFGM and the OFGM (Reprinted with permission of Lockheed Martin Space Systems)

JUNO INSTRUMENTS

JUNO carries nine instruments on-board of the spacecraft, each having a specific scientific purpose on Jupiter. Gravity Science experiment aimed to measure Jupiter's gravitational field and reveal the planet's internal structure. The two magnetometers are to map three-dimensional magnetic fields at Jupiter extremely accurately. The magnetometers will map Jupiter's magnetic field and will provide understanding of the magnetic field nature of the inner parts of Jupiter during the entire mission. The JUNO spacecraft microwave radiometer (MWR) consists of six radiometers designed to measure the thermal radiation from the Jupiter atmosphere beneath the cloud, revealing water content from the deepest level, helping to understand how Jupiter was formed. The six radiometers have six antennas located on two sides of the Juno hexagonal body. The six antennas are connected to a receiver, which sits in the instrument vault on top of the spacecraft. The Jupiter Energetic Particle Detector Instrument (JEDI) measures space high (30 – 1,000,000) KeV energetic particles and Jupiter's magnetic field, while the Jovian Auroral Distributions Experiment (JADE) measures space low energetic particles (0 – 30) KeV charged particles, and operates closely with JEDI. The plasma instrument WAVE measures radio and plasma waves in Jupiter's magnetosphere, to help understand the interaction between magnetic field, the atmosphere and the magnetosphere and activities related to auroras. The Ultra Violet Spectrogram (UVS) will study Jupiter's auroras in ultraviolet light, and together with JADE and JEDI helps understand the relationship between auroras, the streaming particles and the Jupiter's magnetosphere. The eighth instrument, (JIRAM) Jovian Infrared Auroral Mapper is a camera and a spectrometer to study Jupiter's atmosphere in and around auroras, and JUNOCAM, the ninth instrument is to photograph Jupiter's cloud. Figures 3A and 3B show the JUNO spacecraft with its instruments.

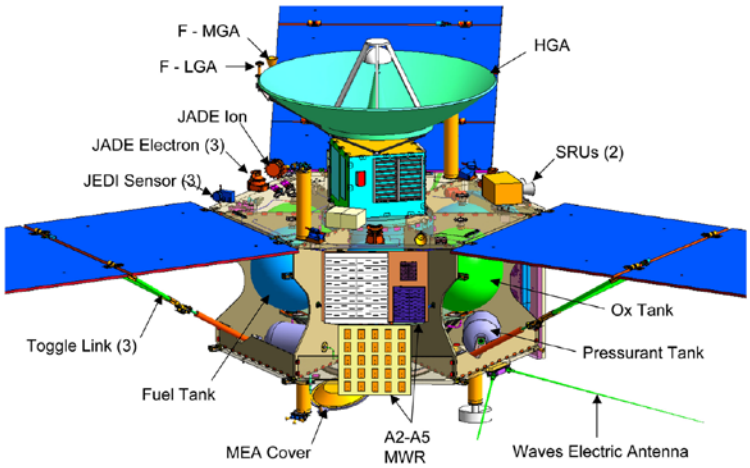

Figure 3A - JUNO Spacecraft and Payload/Instrument Set (Reprinted with permission of Lockheed Martin Space Systems)

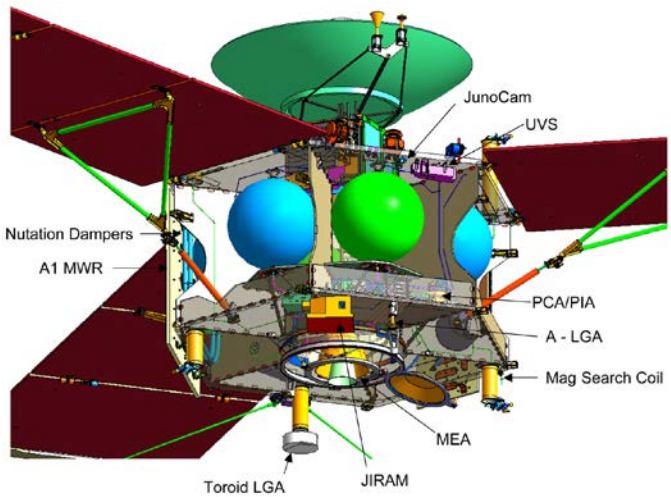

Figure 3B - JUNO Spacecraft and Payload/Instrument Set (Reprinted with permission of Lockheed Martin Space Systems)

JUNO MAGNETIC CONTROL PROGRAM

To minimize the magnetic interference caused by the stray residual magnetic fields, the JUNO Magnetics Control Program (MCP) contained within reference [2] was implemented, and a Magnetics Control Review Board (MCRB) was set up to meet the JUNO mission science requirements. The spacecraft magnetic cleanliness goals were met through maximum allowable magnetic field specifications imposed on the spacecraft engineering subsystems as well as on the JUNO spacecraft science instruments. Early in the project, a magnetics cleanliness control plan based on reference [3] was written and distributed to all JUNO hardware designers. In this document, subsystem design requirements, practices and guidelines on how to minimize magnetic fields within an instrument design were provided. With a requirement of 2 nanoTeslas (nT) at the IFGM location as a basis, all subsystems and assemblies were given an allocated dipole moment requirement. Spacecraft subsystems and science instruments were allocated a dipole moment of 50 Gauss-centimeter^3 (5 nanoTelsa-meter^3), which is equivalent to 10 nT when

measured at a distance of 1 meter. For subsystems consisting of several assemblies, each assembly was allocated a dipole moment of 25 Gauss-centimeter^3 (2.5 nanoTesla-meter^3), or 5 nT at a distance of 1 meter. Components larger than typical subsystems were provided with higher magnetic dipole allocations. These included the solar arrays, high power consuming subsystems such as the power distribution unit, and the propulsion module system. Table 1 below shows a sample set of JUNO magnetic moment allocations for selected instruments. Every JUNO subsystem was allocated a magnetic moment requirement.

Table 1 - JUNO Magnetic Dipole Moment Allocations Sample Set for Science Instruments
(Courtesy of Jet Propulsion Laboratory)

Subsystem/unit	**Magnetic Dipole Moment Allocation (mA-m2 or Gauss-cm3)**
Instruments	
JADE Electronics box	50
JADE Electron sensor +60 deg/+180/+300deg	50
JADE Ion sensor +150 deg	50
UV Spectrometer Electronics box	50
UVS Telescope	50
Waves Electronics Box	50
WAVES dipole antenna w/pre-amp	50
JEDI #1/2/3epd (65/185/295 deg)btw, is	50
Juno Camera Head	50
Juno Camera electronics box	50
Microwave Radiometer electronics	50
MWR Modules	50
MWR Antennas with preamp	50

The goal for JUNO magnetic cleanliness program was to achieve a low and stable residual spacecraft magnetic field at the IFGM and the OFGM locations. Early assessments indicated that these instruments could be compromised due to the multiple number of magnetic source disturbances. This propelled the project to institute a magnetic cleanliness program primarily to ensure that the spacecraft's DC static magnetic fields from its various sources were controlled to less than 2 nT at the IFGM and an AC (variable field) requirement of less than 0.5 nT in a typical magnetic environment of 12 Gauss. To achieve these goals, it was necessary to impose design requirements on all JUNO subsystems and associated hardware, and to test and/or evaluate these subsystems to verify compliance with their respective magnetic requirements. This paper will only concentrate on the efforts implemented to achieve a low and stable 2 nT residual DC magnetic field at the IFGM location.

The magnetics control review board (MCRB) was established to oversee the magnetics cleanliness progress and to promote communication between experimenters and spacecraft subsystem designers, and to facilitate subsystem and system level magnetic assessments, modeling, tests and verification, where necessary. The MCRB consisted of magnetometer science team members, including the principal investigators and co-investigators, members of the Electromagnetics Compatibility Group at the Jet Propulsion Laboratory (JPL), the Aerospace

Corporation (The Aerospace) magnetic specialists, and Lockheed Martin Space Systems (LMSS) EMC engineers. Figure 4 is the MCRB chart with a list of key participants.

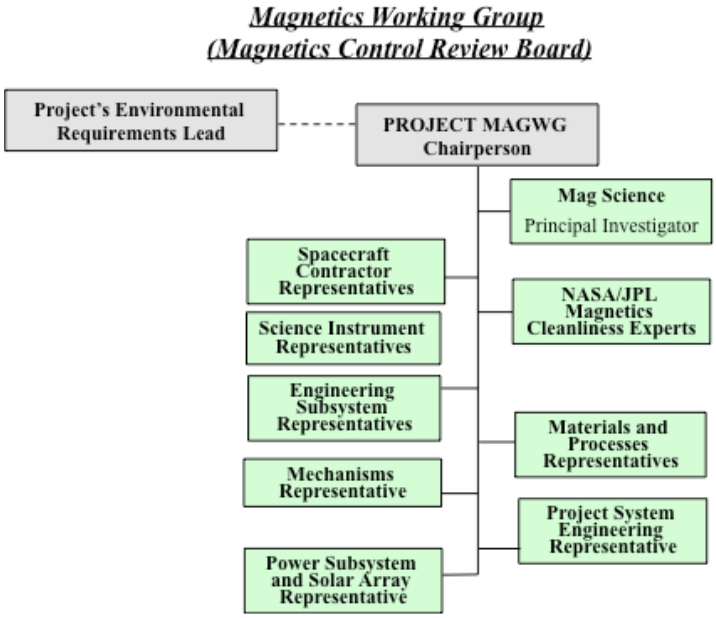

Figure 4 – JUNO Magnetics Control Board Structure (Courtesy of Jet Propulsion Laboratory)

OBSERVATIONS FROM MAGNETIC TEST PROGRAM

Most magnetic cleanliness problems in JUNO mission were due to heritage subsystems. These subsystems were typically designed without much regard to magnetic cleanliness due to the absence of magnetic requirements. To avoid such occurrence on the JUNO project, the MCRB's first priority was to sensitize subsystem designers early in the design process, on the need to maintain a magnetically clean hardware design. All JUNO subsystem cognizant-engineers were informed of their respective magnetics requirements which were contained in the JUNO Magnetics Control Plan. A project-wide magnetic workshop was organized. All spacecraft hardware designers met with members of the MCRB for a full day. At this meeting, participants were made aware of potential magnetic cleanliness problems and the many methods available to solve such problems. Discussed at this workshop were tutorials on when and how to magnetically shield components, implement magnetic moment compensation with permanent magnets, produce battery and system wide wiring layouts with minimum current loop areas, contain stray magnetic flux from motors, modify a design by replacing magnetic materials with suitable and flight acceptable non-magnetic materials, … etc. The designers were encouraged to minimize the use of soft magnetic materials such as invar and kovar as well as hard magnetic materials such as permanent magnets. For example, the use of non-magnetic 300 series stainless steel was encouraged over the more magnetic 400 series stainless steel. A set of guidelines were established that assisted hardware designers in developing the best design, which produced the least amount of magnetic effects. The workshop also recommended that all hardware cognizant-engineers verified the adequacy of their magnetic control design as early as possible by having the design assessed by knowledgeable MCRB members. The workshop heavily emphasized on the importance of assessing magnetic problems as early as possible to allow for flexibility in the available solutions. The MCRB working activities general approach is shown in Figure 5 below:

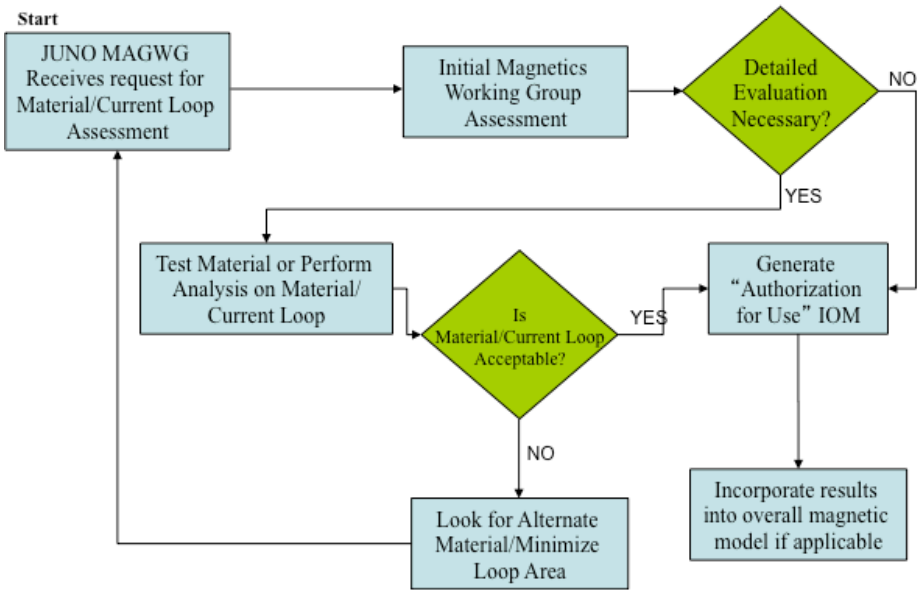

Figure 5 - The overall JUNO MCRB Implemented Magnetic Cleanliness Approach (Courtesy of Jet Propulsion Laboratory)

Based on the MCRB team members efforts, many hardware designers adjusted their respective designs to provide optimum magnetic moment cancellation of magnetic components. For example, in the Radio Frequency Subsystem (RFS), RF waveguide switches and two small Deep Space Transponders were packaged in such a manner that their respective magnetic field polarities were in opposite directions to completely cancel their respective magnetic moments, thus using "self-cancellation approach". The Propulsion subsystem designer arranged all magnetic latch valves in a configuration that provided an optimun magnetic self-cancellation. In many cases where magnetic materials were to be used, similar non-magnetic or less magnetic replacements were used. Another example of self-cancellation was the reduction of fields of all solar array panels. Each solar cell circuit was configured to provde self-cancelling magnetic moments by reversing the current direction in circuit pairs. Where magentic materials could not be replaced, "magnetic compensation approach" was applied such as was the case with the traveling wave tube Amplifier (TWTA), where compensation magnets were mounted near the unit but with opposite polarities.

Many subsystems implemented redesign of their respective wiring layout with the goal of minimizing current loop areas. For example, the battery wiring layout had an original design that generated several hundred nanoTeslas at 1 meter. The battery cell-to-cell wiring design was modified and all loop areas were eliminated by the implementation of cross-strapping cells. The linear boom actuator (LBA) initially had a design that contained magnetic materials; these were replaced with non-magnetic materials. The Main Engine thermal nickel shield, which is a soft magnetic material, was removed and replaced with titanium, and the damping subsystem material was replaced with a non-magnetic material. Figure 6 shows the test set-up for the Main Engine Thermal shield inside the three axis Helmholtz Coil ready for magnetic material testing.

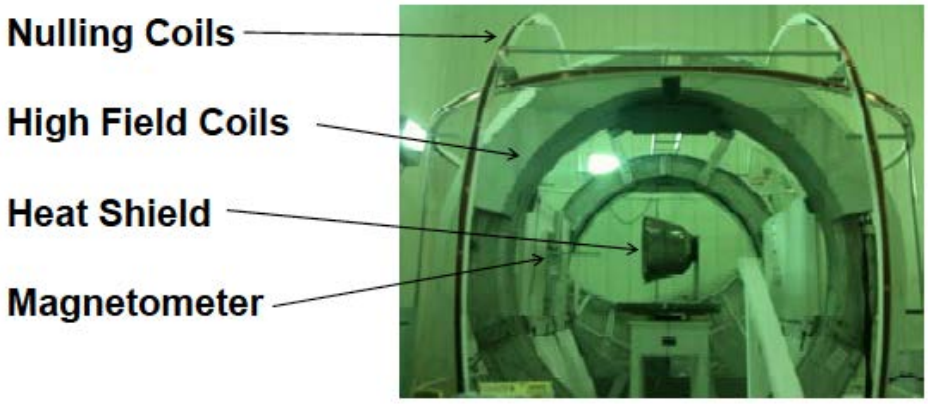

Figure 6- JUNO Main Engine Thermal Shield inside a 3-Axis Helmholtz Coil (Courtesy of Jet Propulsion Laboratory)

Another example, the Radio Plasma Wave Subsystem (WAVES) constructed its antenna mechanisms out of mainly non-magnetic materials, such as titanium, composites, and plastic gears. And, its search coil antenna highly permeable core was reduced to a size that minimized the impact to the magnetometer sensors. In instances where subsystems could not provide self cancellation or materials change, "magnetic compensation" was employed. The most significant magnetic compensation occurred in the latch valves. Propulsion Module System latch valves had the highest dipole moments of any component on the spacecraft. Each latch valve was measured and magnetically compensated by placing them opposite to the magnetic moment of a neighboring latch valve, arranging them for an optimum self-compensation approach. The TWTAs were also magnetically compensated. In order to avoid operational interference, the compensation occurred at a safe distance from each TWTA. For minimum magnetic impact and optimum magnetic compensation, interference and separation between magnetic components in a subsystem magnetic modeling and simulation was used with the magnetic test program.

SUBSYSTEM TEST AND VERIFICATION

To verify magnetic requirements compliance, each JUNO subsystem and assembly was tested and in some cases modeled and magnetically simulated prior to final installation on the spacecraft. Magnetic field measurements were conducted inside a three-axis Helmholtz coil system used to null-out the earth's magnetic field, and therefore provided a zero-field environment to minimize the impact that induced field effects have on the magnetic measurements. Magnetic testing of JUNO subsystems was typically performed early in the development process to allow for design modifications to meet the magnetic cleanliness requirements. In some of the testing, selected subsystems were energized in worst-case power consuming modes to determine the magnetic field due to current flow. Typical magnetic tests consisted of first measuring the subsystem inside a zero-magnetic field environment created by the Helmholtz Coil, demagnetizing the subsystem, and then measuring its residual magnetic field. From the measured magnetic field values, the X, Y and Z axis dipole moments were extracted. The magnetic measurements provided accurate magnetic dipole moment results for each unit tested. Figure 7 are pictures of the magnetic test facilities setup at JPL and Lockheed Martin (LM) used for measuring subsystem magnetic fields.

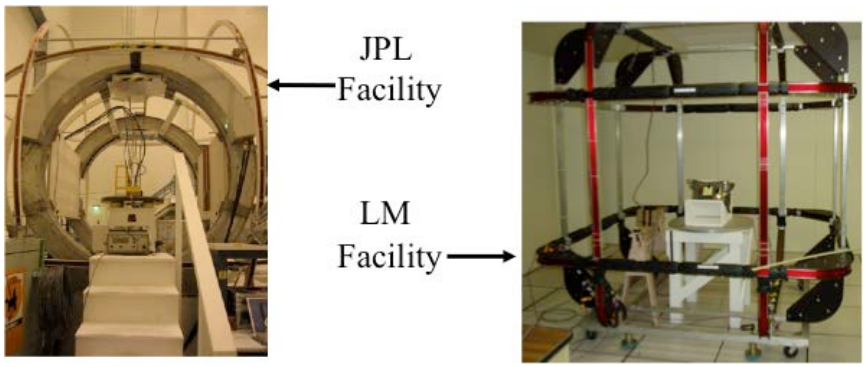

Figure 7 – JUNO Subsystems Magnetic Test Facilities (Courtesy of Jet Propulsion Laboratory, and reprinted with permission of Lockheed Martin Space Systems)

The total residual magnetic field at the IFGM and OFGM locations was calculated by analysis using magnetic dipole moment data from subsystem measurements to verify that the JUNO spacecraft magnetic condition satisfied the magnetic requirement at the sensor locations. Table 2 shows sample results of JUNO payload instruments identified magnetic items and proposed actions for risk mitigation. An overall total of 65 measurements were conducted.

Table 2 – JUNO Subsystems Typical Sample Results (Courtesy of Jet Propulsion Laboratory)

Payload	Identified Magnetic Items	Magnetic Field At 1 Meter	Proposed Action/Comments	Concern Rating
FGM (A, B, electronics)	Magnetic Core	N/A	N/A	Low Concern
ASC elect, A, B	None (lots of brass, silver, gold)	N/A	N/A	Low Concern
JADE Electronics	Nickel plating on connectors, piece parts (mesh etc)	<2 nT in 12 Gauss field	Use as is	Low Concern
UVS	Scan Mirror Motor/magnets Magnets in latch doors Nickel plated parts Stainless Steel 300 series 17-7 PH	 2 nT at 1.8 meters (one mag)	Characterization test plan in place, no issues expected	Low Concern
WAVES	Magnetic search coil core Ferrite beads Toroidal Powder core	228 nT at 12 Gauss < 1 nT in zero field	Reduce core length to acceptable level. Approved by MCRB. Test plan in place for hinge assy/release mech	Low Concern
JEDI	Stainless Steel 300 Series CRES 400 series Nickel plated backshells Nickel grid 17-7 PH Mollypermalloy Powder Core Ferrite-Ferroxcube	<< 1 nT in zero field	Characterization of piece parts performed by APL. No issues uncovered. Use as is.	Low Concern
JIRAM	Motor Stainless Steel 300 Series	2.5 nTo-p at 1 meter	Tests performed by Galileo. Use as is	Low Concern
MWR	Mu-metal shields, isolators, nickel plated chassis Heat treated coax connectors Nickel plated connectors	Small shield <2 nT in 12 Gauss Large 18.6 nT in 16 Gauss << 1 nT in 12 Gauss	Use as is	Low Concern
JunoCam	Small magnetic parts 440C 15-5 PH Electroless nickel plating	Sensor Head <0.06 Gauss @0.5” Electronics <0.16 Gauss @0.5”	Characterized MSL Cam. No issues expected on Juno Cam. Use as is.	Low Concern

At IFGM the spacecraft's magnetic field was calculated by summing all measured subsystems’ extrapolated vector components of the dipolar moment. The extrapolation considered the relative

orientation of the subsystem and the location of the center of mass of the subsystem in terms of spacecraft coordinates. A "sums dipole spreadsheet" was created by JPL using "as received" dipole moments and "demagnetized" dipole moments. The results were then used to model the overall spacecraft magnetic field at the magnetometer sensor locations. Based on the dipole models provided, the overall JUNO's spacecraft's magnetic field at IFGM is provided. Table 3 below shows an example of the JUNO subsystem dipole moment spreadsheet, where the net magnetic sum has been calculated at the upper right hand corner in X, Y, and Z directions and the total dipole moment is determined as follows:

Table 3 – JUNO Subsystem Dipole Moment Spreadsheet and Net Magnetic Sums at IFGM -Partial Example Shown Below. (Reprinted with permission of Lockheed Martin Space Systems)

Error Checking
ok

Mode
DC

Total B field at magnetometer (nT) in SC coordinates			
Bx	By	Bz	Brms
-9.73E-02	-4.39E-02	-5.90E-02	1.22E-01

	Dipole Moments mA-m^2			Results: B field (nT) at magnetometer from DUT			
Name	x	y	z	Bx	By	Bz	Brms from DUT
Battery 1	-9.9	1.2	-2.6	1.083E-04	-1.848E-04	-7.779E-04	8.068E-04
Battery 2	-9.9	1.2	-2.6	9.614E-04	-4.054E-04	-1.241E-03	1.621E-03
CME	-0.2	-3.4	-3.7	7.439E-04	-2.869E-04	3.466E-04	8.694E-04
PDDU	-14.6	-17.4	43.2	-3.312E-03	-4.098E-03	1.898E-03	5.600E-03
PIU	3.1	2.7	6.9	-4.962E-04	3.619E-05	2.181E-04	5.432E-04
JADE Electron Sensor 060	3.2	0.6	-1.3	-2.342E-04	-6.074E-05	1.939E-04	3.100E-04
JADE Electron Sensor 180	3.2	0.6	-1.3	-1.266E-04	1.730E-04	1.231E-04	2.472E-04
JADE Electron Sensor 300	3.2	0.6	-1.3	1.087E-03	-1.082E-04	3.803E-04	1.157E-03
JADE Ion Sensor	2.8	1.9	-0.8	1.868E-04	-7.620E-05	5.943E-05	2.103E-04
JADE Electronics	-1.7	0.7	7.6	-2.118E-03	2.256E-04	1.279E-04	2.133E-03
JEDI Sensor 180	-27.2	8.6	0.7	-4.563E-04	3.079E-04	-1.181E-03	1.303E-03
JEDI Sensor 270	-27.2	8.6	0.7	-1.169E-04	-6.069E-04	-3.378E-04	7.043E-04
JEDI Sensor 90	-27.2	8.6	0.7	7.137E-04	3.659E-05	-3.527E-04	7.970E-04
JIRAM Optics	1.1	4.0	6.3	6.220E-04	-3.495E-04	3.750E-04	8.060E-04
JIRAM Electronics	0.6	2.2	3.8	6.998E-05	-7.340E-04	8.010E-05	7.417E-04
Junocam Optics	-2.2	0.8	-0.1	1.199E-05	5.532E-05	-1.462E-04	1.568E-04
Junocam Electronics	6.8	0.2	-0.2	1.049E-03	-3.903E-04	-8.826E-05	1.123E-03

SYSTEM LEVEL TEST PROGRAM AND RESULTS

After completing the subsystem level DC magnetic field tests and/or analyses and populating their respective dipole moments into the "Dipole Sum model" spreadsheet to allow for the modeling and monitoring of the overall spacecraft dipole magnetic moment and magnetic fields at the IFGM and OFGM sensor locations, three types of system-level DC magnetic tests were performed to validate the overall model and verify system compliance of the magnetic cleanliness requirements. These tests were system rotational test, where the spacecraft was rotated about its vertical axis through 360 degrees, a system translational (pendulum) test, whereby the spacecraft was displaced about a horizontal axis, and a powered (spacecraft completely energized) test, whereby the spacecraft current-induced magnetic fields were measured. This paper will discuss the translational test results as it provides the clearest indication of system compliance to magnetic cleanliness. Results of the system level translational magnetic tests indicated an excellent correlation between measured test data and predictions from the JUNO "Dipole Sums model" spreadsheet. Some minor discrepancies between the

measured data and predictions from the summary spreadsheet were observed, but none that predicted non-compliance with the IFGM requirement for < 2 nT DC and 0.5 nT AC (0-30 Hz) at the magnetometer location. Figure 8 below shows positions of the two sets of magnetic field sensors used during these tests (supplied by JPL and Goddard Space Flight Center) for the JUNO spacecraft translation test.

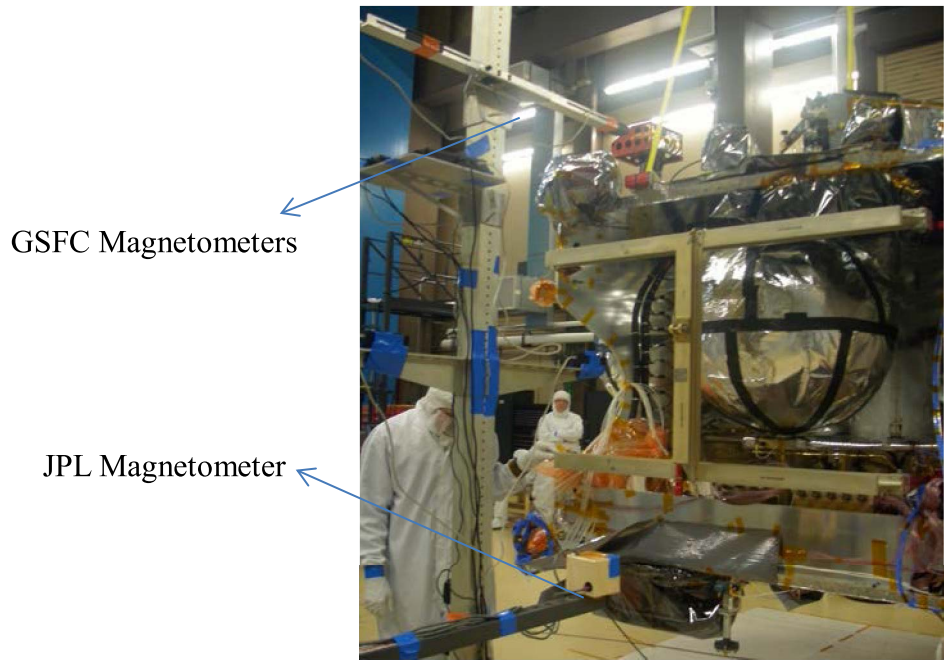

Figure 8 – JUNO Spacecraft Translation Test setup and the detecting Magnetometers Sensor Locations (Reprinted with permission of Lockheed Martin Space Systems)

Table 4 provides a summary of the total system level magnetic fields in X, Y, and Z directions as calculated from the "Dipole Sums model" spreadsheet. These modeling results were then compared against the actual measured results.

Table 4 – JUNO System Dipole Moment Spreadsheet Net Magnetic Sums at IFGM (reprinted with permission of Lockheed Martin Space Systems)

Magnetometer location (m) in SC coord.			Total B field at magnetometer (nT) in SC coordinates			
x	y	z	Bx	By	Bz	Brms
10.026	0	1.7	-0.097	-0.044	-0.059	0.122

SYSTEM TRANSLATION TEST SETUP

In order to capture the magnetic field signature and increase the signal to noise ratio, the test magnetometers were positioned close to the spacecraft and along various spacecraft heights. The

layout for the X-axis translation test is shown in Figure 9.

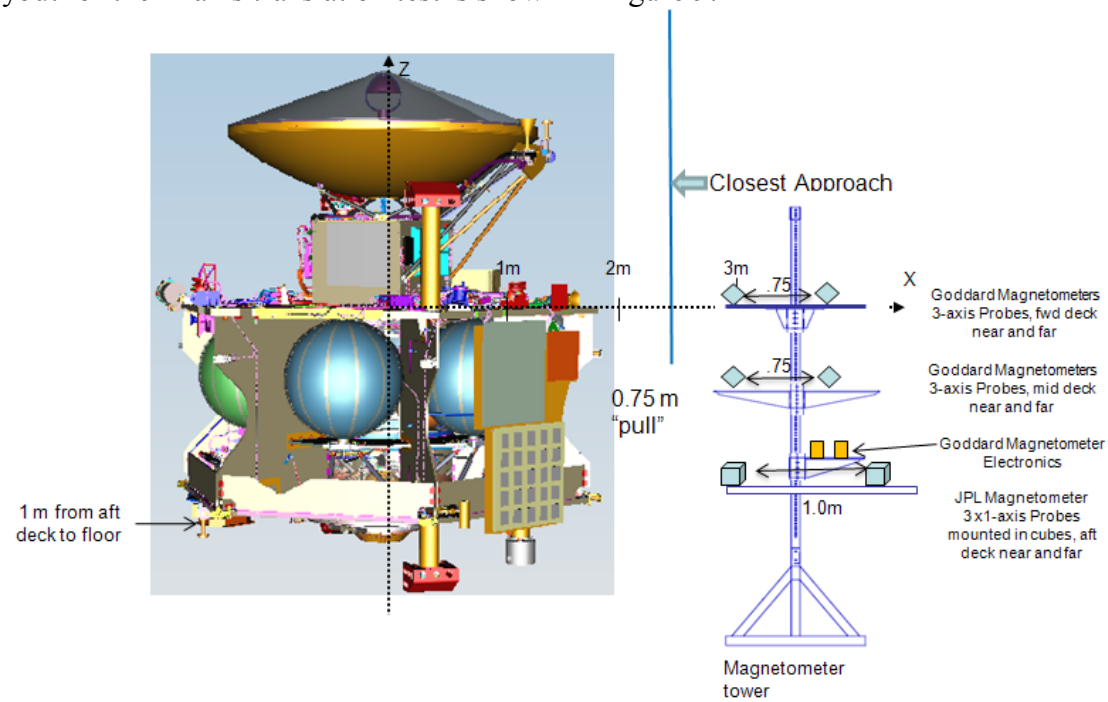

Figure 9- X-axis System Translation (aka Pendulum) Test Set Up (Reprinted with permission of Lockheed Martin Space Systems)

For the X-axis translation test (in the direction of the flight magnetometers locations), the three axis-magnetometer probe array was in line with the +X axis of the spacecraft. For the Y-axis translation test, the three axes-magnetometer probe array was in line with the +Y axis of the spacecraft. One pair of Goddard-supplied 3-axis magnetometer probes ("GSFC Probe Position 1") was aligned with the forward deck, with the near probe at 3 meters from spacecraft center and the far probe at 3.75 meters. Another pair of Goddard-supplied 3-axis magnetometer sensors or probes ("GSFC Probe Position 2") was aligned approximately halfway between the forward and aft decks (0.75 meter below the forward deck), with the near probe at 3 meters and the far probe at 3.75 meters. The JPL single axis probes were assembled into 3-axis magnetometer sensors and aligned with the aft deck ("JPL Position"). The near JPL magnetometer test sensors were at 3 meters and the far sensors were at 4 meters. The absolute magnetometer positions relative to spacecraft, as measured by the laser alignment are given in the following Table 5. The spacecraft translation was always in the magnetic East-West direction to minimize the effects of magnetic fields induced by the Earth's magnetic field.

Table 5 – JUNO System Magnetics Test Magnetometer Sensor Positions (Courtesy of Jet Propulsion Laboratory, and reprinted with permission of Lockheed Martin Space Systems)

Mag Sensor ID	**Magnetometer Locations (meters) In Spacecraft Coordinates**			Locations near spacecraft and agency test magnetometer sensors
	X	**Y**	**Z**	
Magnetometer1	3.054	-0.006	2.549	fwd deck, near (GSFC)
Magnetometer2	3.063	-0.079	1.775	middle, near (GSFC)
Magnetometer3	3.054	0.047	1.046	aft deck, near (JPL)
Magnetometer4	4.049	0.024	1.042	aft deck, far (JPL)
Magnetometer5	3.813	-0.084	1.785	middle, far (GSFC)
Magnetometer6	3.805	-0.004	2.553	fwd deck, far (GSFC)

To initiate the translational test, the spacecraft was pulled 0.75 meter off-center and then released. During the translation motion, a laser positioning device tracked the location of the spacecraft relative to the probes as the spacecraft moved back and forth in a pendulum motion. The magnetometers measured the magnetic signature of the swinging spacecraft for 3 minutes.

ANALYSIS BACKGROUND

Prior to the system test, predictions were performed as to the expected magnetic field results at the selected test magnetometer locations. The predicted data were directly obtained from the JUNO Dipole Sums model. The JUNO Dipole Sums model took all of the data from individually measured subsystems and combined it into a system level model. For the translational test analysis, the sums model was solved in Excel for the spacecraft true position based on the laser positioning data. The sums model predicted the magnetic field for movement along the swing axis only. The prediction uses only the sources that were present for the translation test; solar arrays, linear actuators, etc. were not included.

ANALYSIS SUMMARY RESULTS OF TRANSLATION TESTS

A summary of the translation test results for each probe location is listed in Table 6 below. The magnetic field amplitudes shown in the Table 6 below is the magnitude of the magnetic field of the vector sum of three orthogonal magnetic field sensors at each of the magnetometer probe locations.

Table 6 – Summary of Total Magnetic Field Results for Each Probe Location (Reprinted with permission of Lockheed Martin Space Systems)

Swing Direction	Magnetometer Position	Measured Peak to Trough (nT)	Predicted Peak to Trough (nT)
X-Axis	Forward Deck Near (GSFC Probes)	3.5	3.5
X-Axis	Forward Deck Far (GSFC Probes)	1.0	1.5
X-Axis	Mid Deck Near (GSFC Probes)	3	2.5
X-Axis	Mid Deck Far (GSFC Probes)	2	2.3
X-Axis	Aft Deck Near (JPL Probes)	3.5	1.8
X- Axis	Aft Deck Far (JPL Probes)	1 (noisy)	0.7
Y-Axis	Forward Deck Near (GSFC Probes)	8	3
Y- Axis	Forward Deck Far (GSFC Probes)	2	2
Y-Axis	Mid Deck Near (GSFC Probes)	9	4.5
Y-Axis	Mid Deck Far (GSFC Probes)	2	4
Y- Axis	Aft Deck Near (JPL Probes)	6.2	13.8
Y- Axis	Aft Deck Far(JPL Probes)	1	0.7

The X-axis forward deck results, which are the most relevant since these predict the fields along the magnetometer boom as well as at the IFGM, were extremely well matched. This is especially important, as the magnetometers are located on the X-axis, near forward deck level. The far results generally matched better than the near probe results. Since the IFGM and the OFGM magnetometers are 10 and 12 meters from the center of the JUNO spacecraft, the results provide a positive indication of matching system test versus modeling outputs.

ANALYSIS DETAILED RESULTS

The X-axis data collected during the translational test with the test magnetometers positioned close to the spacecraft forward deck was analyzed and compared against the theoretical magnetic fields from the Dipole Sums model. This data was the most important of all data collected as it provided a thorough understanding of what to expect at the IFGM location along the spacecraft X-axis. Figure 10 displays the X-axis translational measured data versus the predicted results.

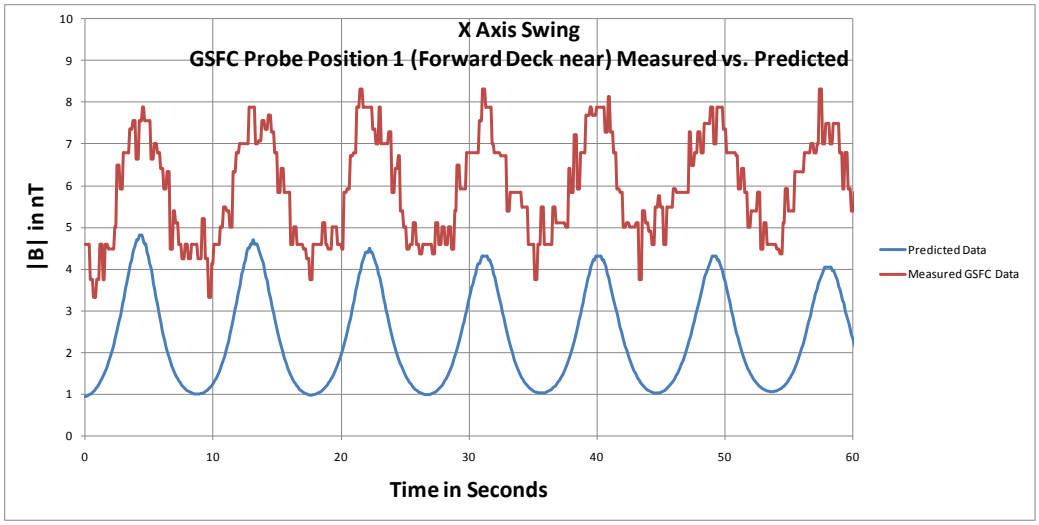

Figure 10 – JUNO System Translation Test Results (From Lockheed Martin Report) (Reprinted with permission of Lockheed Martin Space Systems)

In the above Figure 10, the vertical scale is 1 nT per division. The displayed amplitude is the magnitude of the magnetic field of the vector sum of three orthogonal magnetic field sensors situated near the X-axis forward deck location. The measured magnetic field (red) and predicted magnetic field (blue) are almost identical in amplitude, at approximately 3.5 nT p-p. This shows a strikingly near identical agreement between the predicted results and the actual measurement. The estimated field from these results is about 0.108 nT at the IFGM sensor, compared to the JUNO magnetic Control Plan document limit of 2 nT. The dipoles sum spreadsheet predicted 0.12 nT at the IFGM sensor location. Table 7 below summarizes the results showing a difference of 0.012 nT between the test and the box level system model total magnetic moment at the IFGM.

Table 7 – System Test Results vs System Modeling Results (Courtesy of Jet Propulsion Laboratory)

	Total RSS Magnetic Field At IFGM
System Test Magnetic Results	0.108 nT
System Model From Box Level Moments	0.120 nT
Delta: Test vs Model	0.012 nT

SUBSYSTEM MAGNETIC MODELING, SIMULATION AND ANALYSIS POGRAM

BENEFITS AND APPLICATIONS

Magnetic modeling, simulation and analysis were performed at Aerospace. It fell under the MCRB activities, as part of the JUNO magnetic cleanliness program, and was reviewed and assessed in relation to the JPL magnetic test program. Modeling, simulation and analysis were developed, from early in the project phase, to help the project identify the nature of the magnetic part and component, field strength, distributions around the magnetically sensitive regions, and to cost effectively, mitigate the risk of magnetic interferences, and remnant magnetization at the

10 meters away at the IFGM, before setting up expensive test programs. Magnetic modeling and simulation was developed, as needed, for spacecraft's subsystems and science instruments in zero Gauss, 12 Gauss or 50 Gauss external applied magnetic fields in X-, Y-, and Z- directions. Wherever it was difficult to verify the magnetic cleanliness through testing, magnetic modeling and simulation has provided qualitative and quantitative inspections and performance verifications. Field strength at 10 meters away at the position of the IFGM was determined through extrapolation of the simulated data. The magnetic modeling and simulation program started with review and assessment of the flight system materials list, and followed the JUNO project Environmental Guidelines and Practices as set by the project in reference 2.

Magnetic modeling, simulation, and analysis were developed for every level of the JUNO spacecraft hardware and science instruments, from materials to the whole flight system as shown in Figure 11.

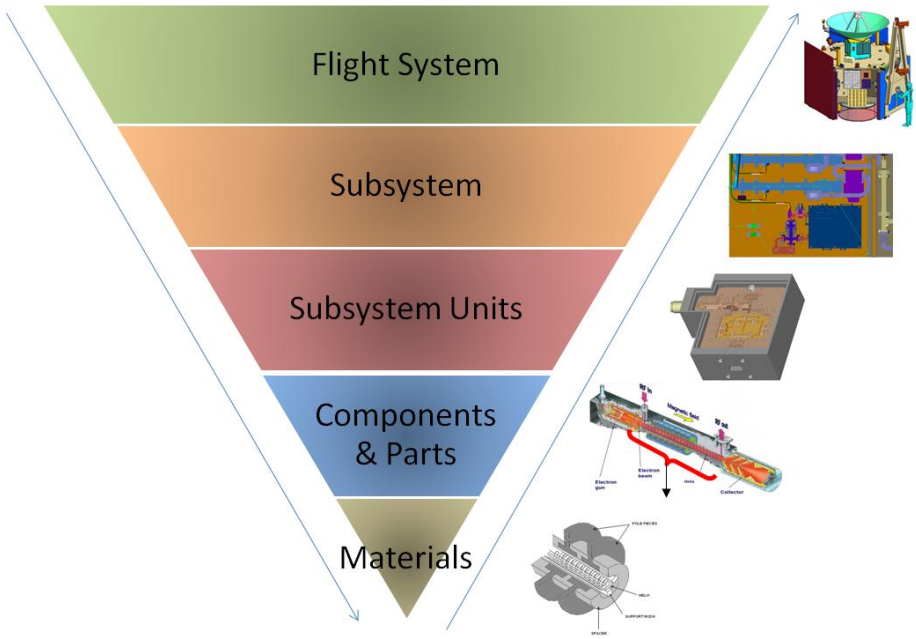

Figure 11 - Magnetic Modeling, Simulation and Analysis Applied to JUNO Mission (© The Aerospace Corporation, 2012)

In this paper we will limit our discussions to presenting modeling and simulation results developed for only three representative examples; the spacecraft telecom subsystem consisting of several magnetic inclusions of samarium cobalt (SmCo5) permanent magnets as compensation magnets and collector magnets, and highly sensitive magnetic component of TWTAs; the science experiment Ka- band translator system (KaTS) solid state power amplifier (SSPA) unit housing made of KOVAR soft magnetic material; and the two magnetically shielded inertial measurement units (IMU)s field interference with one of the science experiments, the Microwave Radiometer (MWR) electronic box within the spacecraft attitude control subsystem (ACS).

REQUIREMENTS AND APPROACH

JUNO modeling and simulation required using the commercially available three dimensional (3D) Maxwell v12 software package from Ansoft Corporation. Magnetostatic, Eddy current or transient electromagnetic analyses were performed depending on the application. Engineering drawings helped define the geometry of the components to model, and knowledge of the material specification and assignment of the material's properties to solid components in the model identified the magnetic environment to be simulated. Effects such as applied external magnetic fields were included in the simulations on "as needed" basis, to correctly simulate the parts' behavior. Fields at a 10 meter away were extrapolated from the simulation and fitted to $1/r^3$ behavior. The schematic workflow structure of how the modeling and simulation was performed is shown below in Figure 12. In this example the process is applied to modeling and simulation of the telecom subsystem in zero external applied fields.

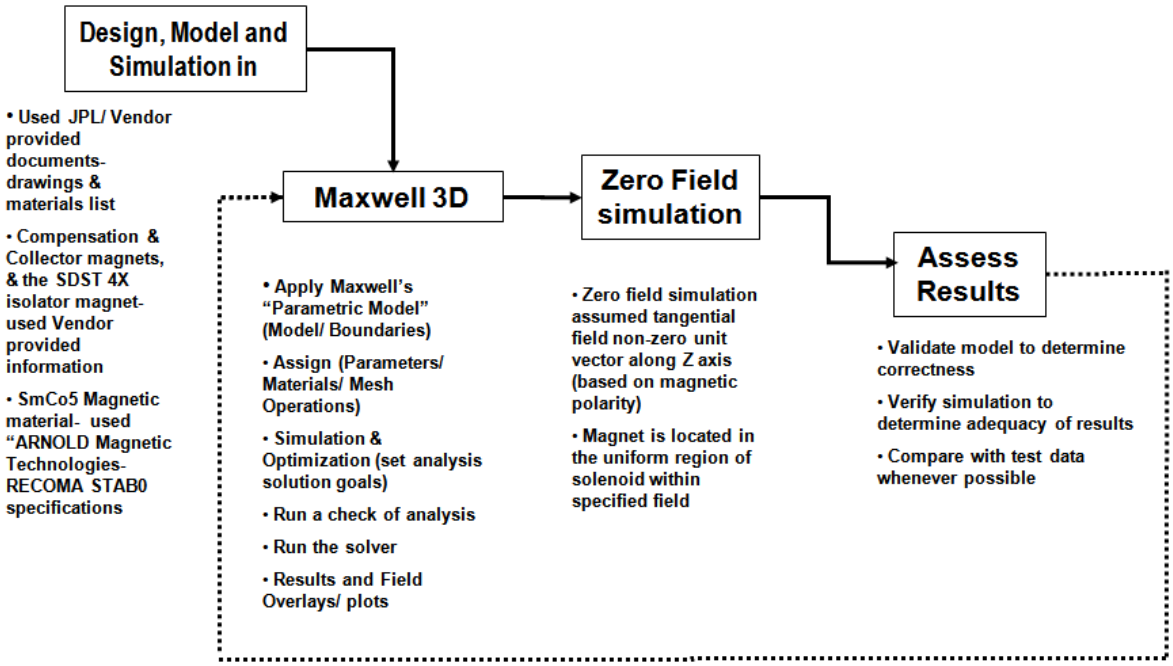

Figure 12 - Aerospace Adopted Schematic Workflow Structure- Example Applied to the Telecom Subsystem (© The Aerospace Corporation, 2012)

EXAMPLES OF MAGNETIC MODELING AND SIMULATIONS

MODELING AND SIMULATION OF THE TELECOM SUBSYSTEM

JUNO telecom subsystem consisted of modeling and simulation of its magnetic inclusions, individually and collectively. The purpose was to determine the field strength, distribution, interferences and influences of each magnetically sensitive part and component to each other and to the neighboring spacecraft other subsystems within 50 cm cubic volume. The geometric position of the magnetic parts within the simulated environment with respect to each other is shown in Figure 13 below.

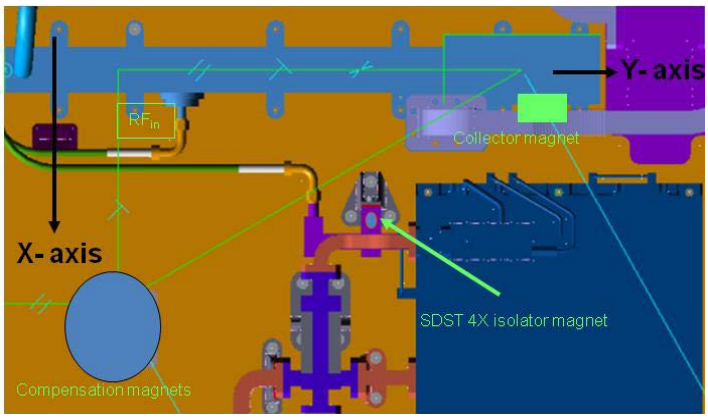

Figure 13 - JUNO Telecom Subsystem with all Magnetic Parts (Courtesy of Jet Propulsion Laboratory)

Magnetic parts and components of the telecom subsystem used for modeling and simulation were; one TWTA Focus magnet consisting of 44 pole pieces and spacers magnets, of iron and stainless steel (SS); one Collector magnet of (20x15x5) mm^3 samarium-cobalt ($SmCo_5$) permanent magnet placed at 25 mm above the center line of the Focus magnet and at 29 mm away from its one end; two Compensation magnets also of (20x15x5) mm^3 $SmCo_5$, in opposite polarity to the Collector magnet, placed at 15 cm away from the opposite end of the Focus magnet; and a stack of two 6.4 mm diameter permanent magnets within the small deep space transponder (SDST)'s 4X multiplier's isolator, which is placed at nearly 11 cm away from half length of the Focus magnet on the same side of the Compensation and the Collector magnets.

Modeling and simulation of the 25 Watt Thales TWTA Focus magnet in zero external applied field consisted of modeling and simulation of 44 pole pieces and spacers, which were of Iron and Stainless Steel (SS) magnets arranged in a format as shown in Figure 14. The 44 magnets were modeled according to the vendor's provided engineering drawings specifications. Figure 14-A shows modeling of the 44 pole pieces and spacers' magnets in the (3D) Maxwell v12 environment. Poles of the 44 magnets were arranged to be (South-North-North-South-South-North-North-South…) based on the vendor's provided specifications also. Applying the magneto-static analysis, The DC magnetic field simulation was developed for the 44 pole magnets in zero externally applied magnetic fields in XY plane at Z=0, as it is shown in Figure 14-B. The insert in Figure 14-B shows a close look to the magnetic field contours in (Tesla) in XY Plane along the surface of the Focus magnet, where magnetic minima and maxima are due to the poles sequencing.

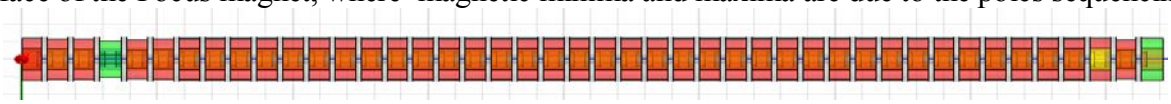

XY Plane View of 44 Piece Magnet Stack

Figure 14-A Thales TWTA Focus Magnet Modeling Effort in Maxwell 12 Environment (© The Aerospace Corporation, 2012)

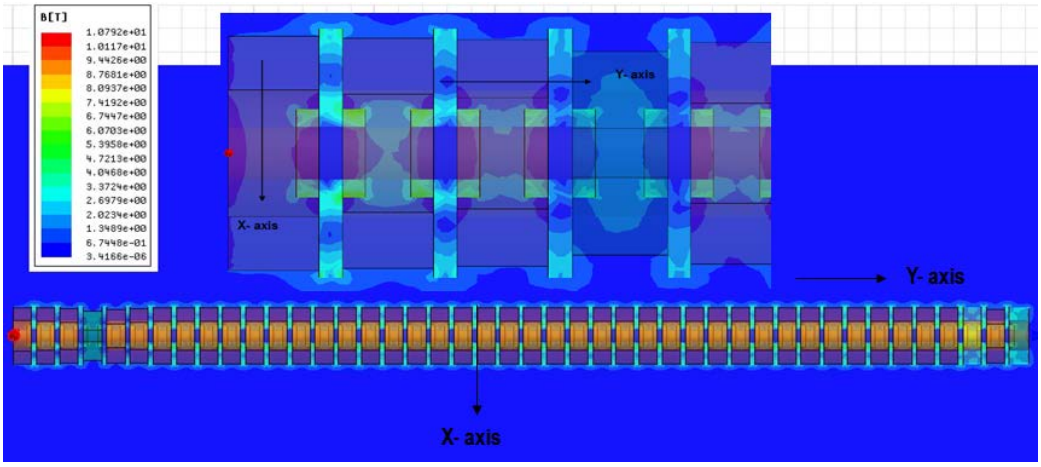

Figure 14-B Magnetic Field (Tesla) Contours in XY Plane on the Surface of the Focus Magnet (© The Aerospace Corporation, 2012)

Next, a Collector magnet of (20x15x5) mm^3 $SmCo_5$, a 1.4 Tesla permanent magnet, was added to the Focus magnet at a 25 mm above the center line of the Focus magnet and at a 29 mm away from one end of it. Using the magnetostatic module, Figure 15 below summarizes the simulation results at a 30 cm distance along the Focus magnet in the Y- direction. Over the length of the Focus magnet the field strength varied between 1000 Gauss on the surface of the magnet to (3 to 4) Gausses at 20 mm or 30 mm above the magnet. Moving away from the Focus magnet, field values of 1.4 Tesla were detected at the Collector magnet position and field interferences of as high as (20 to 30) Gauss at 30 cm away were observed which was considered high and not acceptable by the magnetic cleanliness program. This simulation helped the project to reduce the number of tests performed on the TWTA units

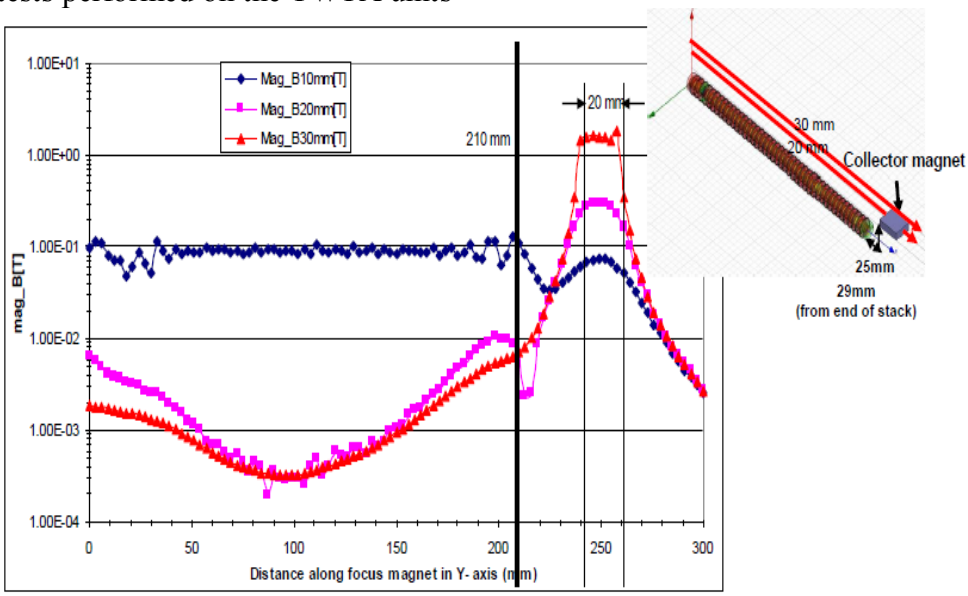

Figure 15 - Field Variation Over the Length of the TWTA Focus Magnet and the Collector Magnet Assembly at 10 mm, 20 mm and 30 mm Above the Surface of the Focus Magnet (© The Aerospace Corporation, 2012)

The simulation results above used to determine the magnetic dipole moment of the TWTA unit, and compare the results with the magnetic dipole moment obtained from the test program. A very good agreement was found. The total magnetic moment of the TWTA M_{total} obtained from the test program was 868 Gauss-cm^3, whereas the deduced magnetic moment from the simulation was (600 $<M_{tot}<$ 1000) Gauss-cm^3. The simulated fields along the Z direction at 10 mm, 20 mm, and 30 mm above the Focus magnet were also compared with those from the test program. The results, which are in agreement, are shown in Table 9 below.

Table 9- Simulated Magnetic Field at 10 mm, 20 mm and 30 mm above the Focus Magnet along +Z- Direction Compared to those Obtained from the Test Program (© The Aerospace Corporation, 2012)

Along +Z- Direction		
Above Focus Magnet	**Simulated B_{tot} with Collector Magnet**	**Calculated B_{tot} from Test Data**
mm	**Gauss**	**Gauss**
10	~2000	1735.52
20	100	216.94
30	50	64.28

Furthermore, a stack of two 6.4 mm diameter permanent magnets of the (SDST)'s 4X multiplier's isolator was added to the assembly. This stack of magnets placed half way along the length of the Focus magnet at 11 cm away. To minimize magnetic interferences from all these magnetic parts, two Compensation magnets, each of 1.4 Tesla, (20x15x5) mm^3 $SmCo_5$ permanent magnet, were placed in opposite polarity to the Collector magnet, and at 15 cm away from the opposite end of the Focus magnet on the same side of the 4X multiplier isolator magnet. Modeling and simulation of this magnetic assembly is shown in Figure 16 below for a 50 cm cubic volume.

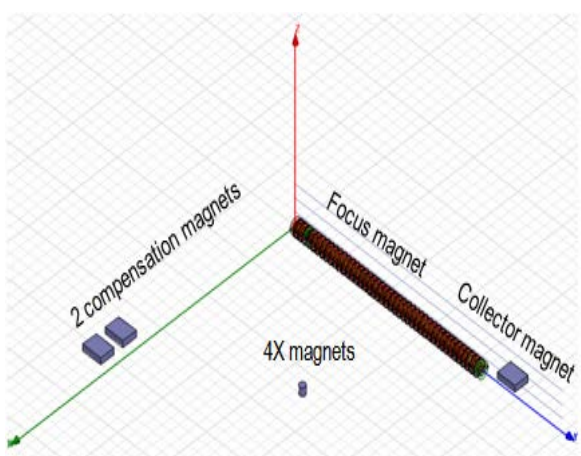

Figure 16-A - JUNO Telecom Subsystem Magnetic Inclusions Positions with respect to each other (© The Aerospace Corporation, 2012)

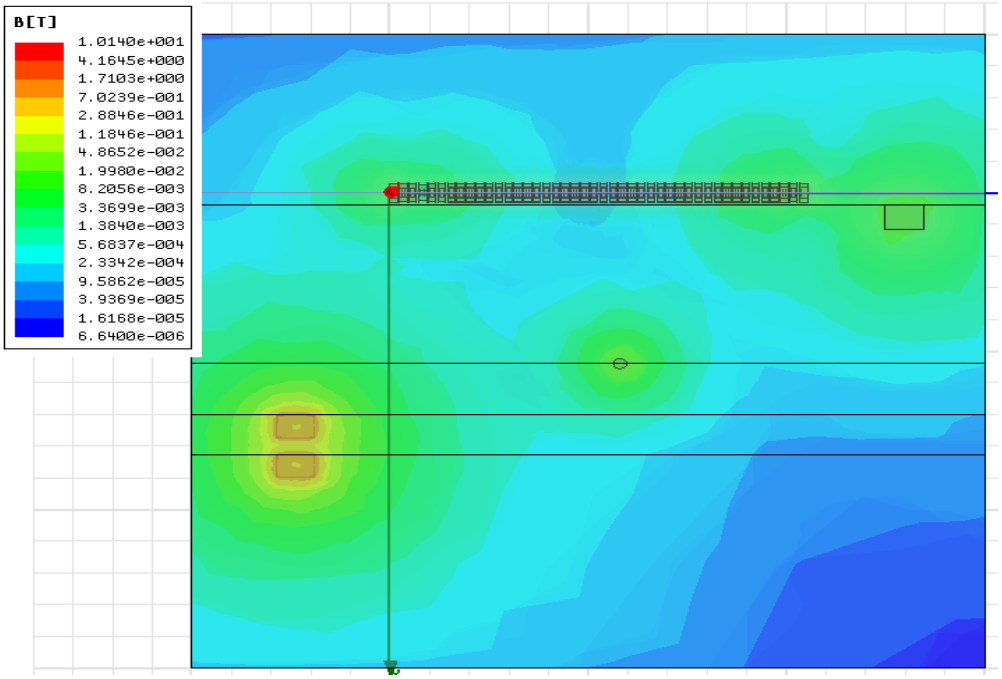

Figure 16-B - Modeling and Simulation of the JUNO Telecom Subsystem Magnetic Inclusions (© The Aerospace Corporation, 2012)

Figure 16-A shows the modeling of these magnets in the (3D) Maxwell v12 environment, whereas Figure 16-B shows the simulation results in XY plane at Z=0. This simulation was developed for zero applied external fields. The field contours in the region represent magnetically weak and intensive areas, field distributions, and interferences among the different magnetic parts in the plane of observance. These results varied above and below Z=0 position and in applied fields of 12 Gauss. The JUNO project used this result to magnetically shield the telecom subsystem remnant magnetization obtained from testing program to minimize the magnetic effects on the neighboring spacecraft subsystems.

The modeling and simulation of the Compensation magnet of 1.4 Tesla, (20x15x5) mm^3 $SmCo_5$ permanent magnet is shown below in Figure 17 for zero applied external fields. The simulation developed over a volume of 30cm x 30cm x 30cm cubic space, where the two TWTAs were to be placed. Field strength and distribution around the magnet were determined.
The simulated magnetic field contours in XY, XZ, and YZ planes as shown below in Figure 17, as well as the magnetic polarity North Pole (N) and South Pole (S) of this material and the field strength over 30 cm cubic volume.

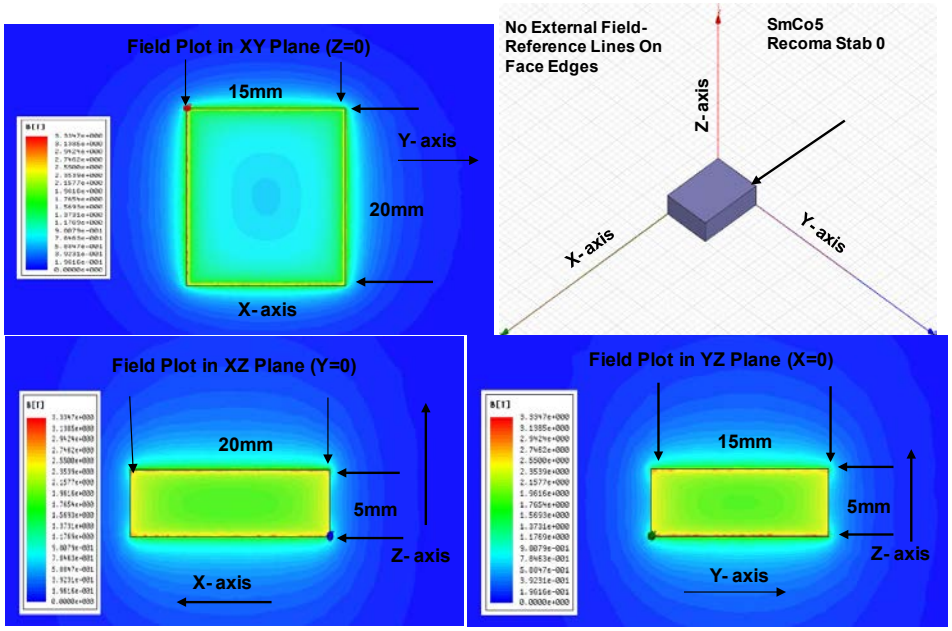

Figure 17- Magnetic Field Distribution and Strength around the Compensation Magnet of samarium-cobalt ($SmCo_5$) Permanent Magnet (20x15x5) mm^3 (© The Aerospace Corporation, 2012)

This magnetic part was also modeled and simulated in 12 Gauss and 50 Gauss applied DC fields in X-, Y-, and Z- directions. The summary results are shown in Figure 18. These results helped the magnetic cleanliness program to identify the strength of the field around this piece at 30 cm, 50 cm, 1 meter and 10 meter away.

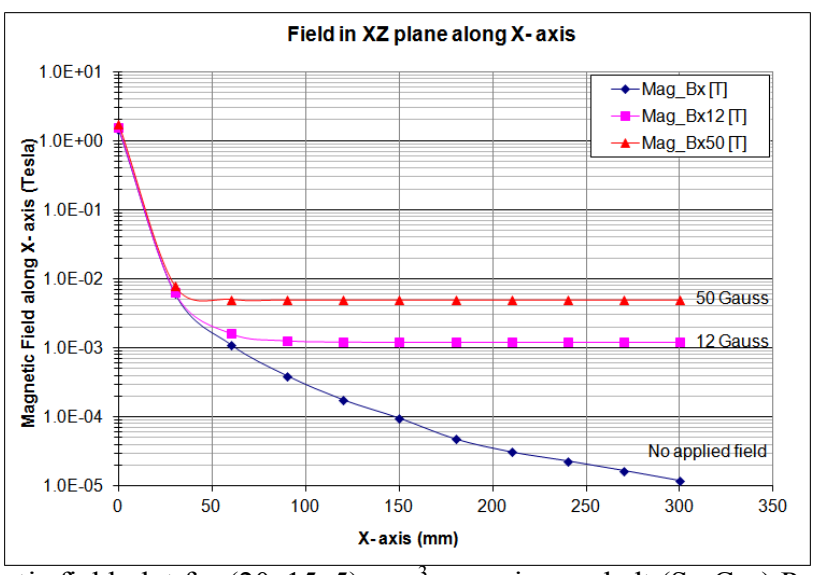

Figure 18- Magnetic field plot for (20x15x5) mm^3 samarium-cobalt ($SmCo_5$) Permanent Magnet in No Applied External Field, and in 12 Gauss and 50 Gauss applied fields in X- direction (© The Aerospace Corporation, 2012)

MODELING AND SIMULATION OF HIGH PERMEABILITY KOVAR USED FOR SOLID STATE POWER AMPLIFIER (SSPA) UNIT HOUSING IN THE KATS TELECOM SUBSYSTEM

The high permeability and soft magnetic material KOVAR is an alloy of Fe(54%)-Ni(29%)-Co(17%)-C(0.02%)-Si(0.20%)-Mn(0.30%) with low coefficient of expansion similar to those of glass and silicon, and thermal characteristics similar to those of alumina. Its saturation Flux Density-Bs~17000 Gauss, and Relative Permeability is 1000 at low fields reaching a maximum of 3700 at 0.7 T (7 kGauss). KOVAR was the housing material for the solid state power amplifier (SSPA) unit used for the science experiment Ka-band translator system (KaTS). Because of the soft magnetic nature of KOVAR, any small change in applied magnetic fields, this unit housing can be magnetized and remained magnetized until the external field is removed. To identify the field strength and distribution around and over 10 meter away from this unit, and how much this unit can contribute to the total magnetic field at the 10 meter away, the SSPA housing made of KOVAR, was modeled and the field simulated with and without 12 Gauss external applied fields in X-, Y- and Z- directions, and the results extrapolated to 10 meters. Figure 19 below shows an example of the simulation for the field around the unit with 12 Gauss external field applied in the Z- direction.

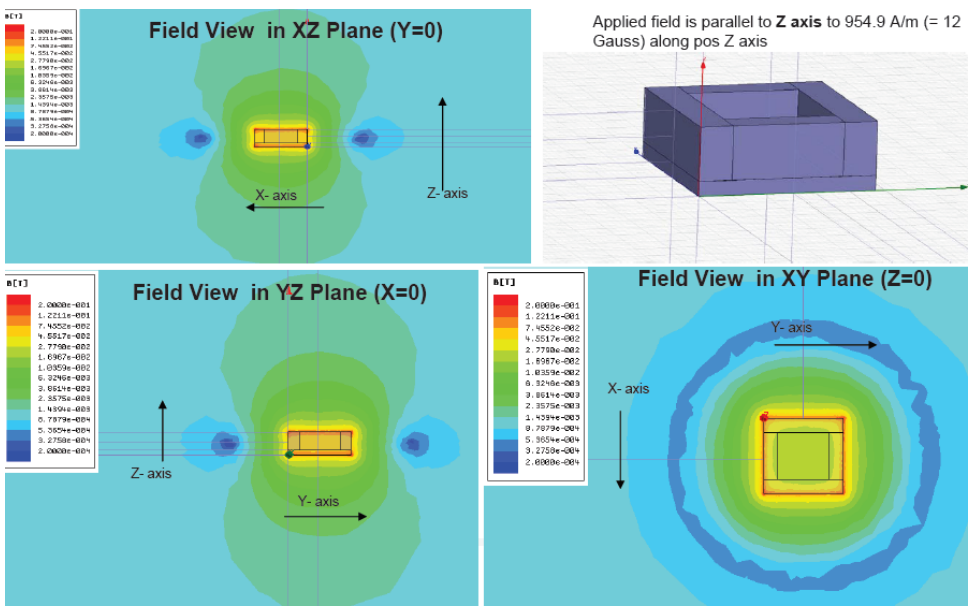

Figure 19 - SSPA Hybrid –Kovar Magnetic Simulation in 12 Gauss Applied Field along Z-axis
(© The Aerospace Corporation, 2012)

And, to determine the field at the 10 m away along the X- direction (at the IFGM) the data were extrapolated and fitted to $1/r^3$ function in XZ plane. Figure 20 shows the extrapolated and the fitted data to 10 meter in zero Gauss applied field. The field dropped to fractions of a nanotesla (0.65 nT) at 10 meter. This result was acceptable by the project and helped the test program as well as to learn about the contribution of the SPPA unit to the total magnetic field at the IFGM, which was below the 2 nT requirement.

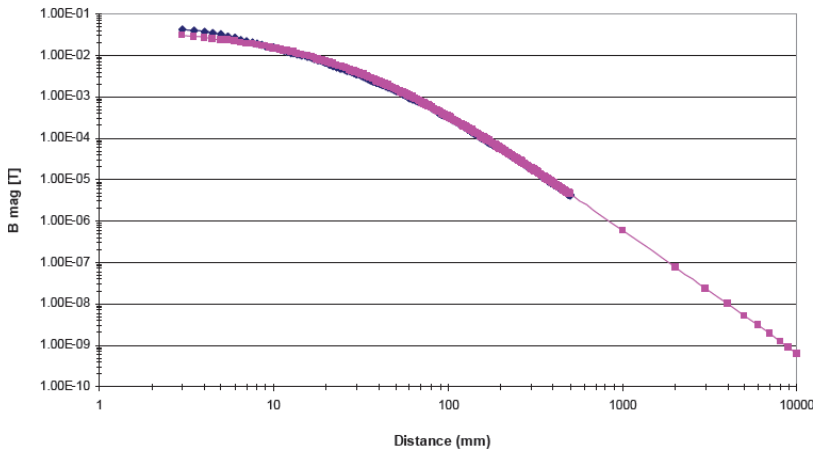

Figure 20 - XZ plane field distribution in Zero Gauss applied field of the SSPA unit along X-axis (Y=0, Z=0) simulated and fitted to $1/r^3$ field. Data extrapolated to 10 m- (© The Aerospace Corporation, 2012)

MODELING AND SIMULATION OF TWO MAGNETICALLY SHIELDED INERTIAL MEASUREMENT UNIT (IMU) IN THE VICINITY OF MWR ELECTRONICS BOX

The MWR electronics box was placed close to two shielded IMUs. The IMU shield material was a high permeability mu-metal, with thickness of 0.02 inch. The diameter of the shielded IMU disc was 4.8 inch and a width of 2.72 inch, while the two shielded IMUs were separated by nearly one inch. The closest IMU was one inch away from the MWR electronics box, the assembly is shown in Figure 22 below. The magnetic cleanliness program required to determine the level of field strength, distribution, and interference of the IMUs on the MWR electronics box as well as at 10 meter away at the IFGM sensor. The modeling and simulation generated a 3D view of the field strength and distribution around the IMUs in the vicinity of the MWR electronics box. Figure 21 Part A is the field simulation around the IMUs, whereas, Part B shows that the field strength and variations at the center of the two IMUs are around 50 Gauss.

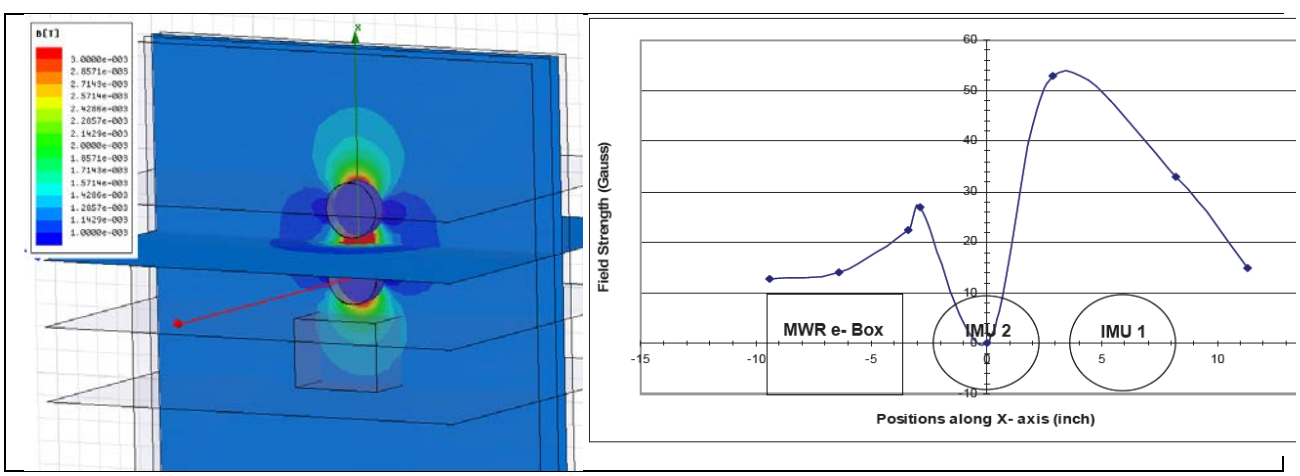

Figure 21 - Modeling and simulation of the two magnetically shielded IMUs (Part A, left; Part B, right) (© The Aerospace Corporation, 2012)

The Mu metal shields the IMU very well. Field inside the shield is ~10^{-6} Tesla with respect to the outside shield area. The field distribution outside the shields across horizontal planes between the shields and the MWR box assembly, along its X-axis center line, varies as follows; less than 40 Gauss above 1st IMU shield, nearly 40 Gauss between the 1st & 2nd IMU shields (1/2 way through), 14 Gauss between 2nd IMU shield and MWR box (1/2 way through), 10 Gauss over surface of MWR box, 2 Gauss across MWR box, <2 Gauss below the MWR box. Field distribution is homogenous over XY, YZ & XZ planes in a spherical area around the 2 shields and the MWR box. The field at 10 meter away, at the IFGM position, was deduced to be a fraction of the 2 nT requirement. These results helped the program to shield the IMUs to protect the MWR electronics box from induced magnetic interferences.

CONCLUSIONS

The JUNO magnetic testing program in conjunction with the magnetic modeling and simulation efforts played an essential role in assessing potential magnetic cleanliness problems early in the project lifecycle. Through the methods of magnetic compensation, judicious material selection (hard vs soft magnetic materials), self-compensation of multiple magnetic parts, current loop area reduction, and magnetic shielding were all instrumental in meeting the magnetic cleanliness requirements imposed on the project. The overall spacecraft requirements of 2 nT static field and 0.5 nT variable field at the IFGM 10 meters away along the X- direction in 12 Gauss were met as verified in the system level tests performed at Lockheed Martin.

The overall efforts of the magnetic control program included the participation of key personnel from each of the spacecraft subsystems (power, propulsion, instruments, attitude control, mechanical, RF telecom) as well as from the Magnetics Control Board members, which included the magnetometer and plasma wave search coil Principal Investigators. The magnetic mapping, modeling and simulation of 65 JUNO subsystems were carried out over several years and at various locations. Early risk-reduction testing as well as qualification testing was conducted at the JPL magnetics test laboratory located in Pasadena, California. The modeling and simulation was performed by the Aerospace Corporation. In addition, subsystem and system level dipole tests, analysis, optimization, and data mapping were performed by Lockheed Martin Space Systems Company in Littleton, Colorado. The JUNO magnetic control program was deemed to be very successful in efficiently controlling the magnetic moments from the 65 magnetic units. Each JUNO spacecraft subsystem made significant contributions which were necessary to achieve the cleanliness goals set out the by the Magnetics Control Review Board Team. The resulting efforts have paid off for the magnetometer science team. Due to the special magnetic control techniques, the extremely careful magnetic design and construction the JUNO spacecraft resulted in the in-flight magnetometer data showing minimal residual fields that have been low and stable, resulting in minimum corrupted scientific data.

ACKNOWLEDGEMENT

The test program work described in this paper was carried out at the Jet Propulsion Laboratory, California Institute of Technology, under a contract with the National Aeronautics and Space Administration. The modeling and simulation work was carried out at the Aerospace Corporation, under a contract with the Jet Propulsion Laboratory, JUNO project management. Acknowledgements go to Dr. Jack Connerney, JUNO magnetometer principal scientist from NASA/ Goddard Space Flight Center, Briand Lessard, Doug Westbury, Bruce Curry and Angela Adams of Lockheed Martin Space Systems, Littleton, Colorado.

REFERENCES

1) http://www.nasa.gov/mission_pages/juno/spacecraft/index.html
2) Juno, Electromagnetic Environmental Effects (E3) Control Plan, Contract Number: 1278766, Document No. Juno–PN-06-0054, SDRL ER-002, Item 001C, Revision: C. May 2008.
3) The Design, Construction and Test of Magnetically Clean Spacecraft – A Practical Guide, Mario Acuna, Laboratory for Extraterrestrial Physics, Goddard Space Flight Center, Greenbelt, MD 20771, Rev. 3.0, October 2004.

BIOGRAPHIES

Mary Boghosian is currently working at the Aerospace Corporation since 2006 within Civil and Commercial Program Office, Planetary and Robotic Missions Group as Project Engineer and Specialist in Magnetics. Prior to joining the Aerospace and participating in the JUNO magnetics cleanliness program, she spent eight years at the Jet Propulsion Laboratory, where she lead successful flight instrument and technology proposals, participated in Advanced Projects Design Formulation Phase studies, developed and patented new concepts for space application magnetic sensor and actuator, and provided support to various flight projects including design, development, and test of the CloudSat quasi-optical transmission line (*QOTL)* 94GHz receiver (flight unit and engineering model) magnet and the housing. She also has extensive experience in design, development and test of cryomagnetic and superconducting magnet systems. Dr. Boghosian holds a PhD in physics of magnetic materials from Imperial College, London University, and MBA from Rensselaer Polytechnic Institute.

Pablo Narvaez is currently working at the Jet Propulsion Laboratory since 1985 in the Mission Environments Group as an Electromagnetic Compatibility (EMC) engineer. Besides participating in the JUNO spacecraft magnetics cleanliness program, he was also involved in the Galileo, Cassini and Ulysses magnetics cleanliness efforts. Mr. Narvaez holds a BS in electrical engineering from University of California, Los Angeles and an MSEE from California State University, Los Angeles.

Dr. Ray M. Herman has over 30 years experience in RF and microwave electronic circuits, particularly RF integrated circuits. Dr. Herman has worked at several aerospace companies and small start-up companies developing commercial electronics. He is the inventor of several patents, and author of several published technical papers. Dr. Herman has a BS, MS, and Ph.D. in Physics, all from the University of Illinois, and did postdoctoral research at Brown University.